Supplementary Materials for

Biomimetic multifunctional electronic hair sensor

Ya-Feng Liu, Pei Huang, Yuan-Qing Li, Qun Liu, Jiang-Ke Tao, De-Jian Xiong, Ning Hu, Cheng Yan, Hao Wang, Shao-Yun Fu

The PDF file includes:

- Fig. S24. Schematic showing of hair shaft deformation under an applied force *F*.
- Fig. S25. Schematics of the structure of hair cells and parameters.
- Table S1. Comparison of the present EH sensor with existing hair sensors.
- Movie S1. Visualized pressure indicator.
- Movie S2. Visualized airflow indicator.

Note S1. Detailed derivation of stress distribution

According to the mechanical equilibrium, when a force is applied to the hair shaft, a pressure (*P*) and a moment (*M*) will be generated around the hair root. As shown in Fig. 1B, when the pressure is perpendicular to the half plane, the state of stress at any point is expressed as [S1]:

$$\begin{cases} \sigma_\rho = -\dfrac{2P\cos\theta}{\pi\rho} \\ \sigma_\theta = 0 \\ \tau_{\rho\theta} = \tau_{\theta\rho} = 0 \end{cases} \tag{S1}$$

where ρ and θ are polar radius and polar angle, respectively. Upon coordinate transformation, the stress (σ_x^P) in the x direction is expressed as:

$$\sigma_x{}^P = -\frac{2P}{\pi}\frac{x^3}{(\mathrm{x}^2+\mathrm{y}^2)^2} \tag{S2}$$

where x and y are abscissa and ordinate, respectively. When the half plane is under moment (*M*), the state of stress at an arbitrary point can be expressed as:

$$\begin{cases} \sigma_\rho = \dfrac{2M\sin 2\theta}{\pi\rho^2} \\ \sigma_\theta = 0 \\ \tau_{\rho\theta} = \tau_{\theta\rho} = -\dfrac{M(\cos 2\theta + 1)}{\pi\rho^2} \end{cases} \tag{S3}$$

After coordinate transformation, the stress (σ_x^M) in the x direction is expressed as:

$$\sigma_x{}^M = \frac{8M}{\pi}\frac{x^3 y}{(\mathrm{x}^2+\mathrm{y}^2)^3} \tag{S4}$$

P is arbitrarily supposed to equal 0.1 N and M is assumed to equal 0.1L N.mm. The schematic of distributed force is presented in Fig. S22. The distributed force (q_1) at the fixed end section of the hair induced by concentrated force is expressed as [S2]:

$$q_1 = \frac{P}{S} = \frac{0.4}{\pi d^2}$$

where S is the cross sectional area of the hair and L is the length of hair. The distributed force (q_2) at the fixed end section of the hair induced by pure moment is expressed as[S2]:

$$q_2 = \frac{M}{I}\eta = \frac{6.4L}{\pi d^4}\cdot\eta$$

where I and η are the moment of inertia and the distance from the point M(x, y) to the origin of the coordinate on the AB line, respectively. The total distributed force q(y) at the fixed end section of hair is expressed as:

$$q(\mathrm{y}) = q_1 + q_2 = \frac{0.4}{\pi d^2} + \frac{6.4L}{\pi d^4}\cdot\eta \tag{S5}$$

The stress (σ_x) in the x direction is expressed as:

$$\sigma_x = -\frac{2P}{\pi}\frac{x^3}{(\mathrm{x}^2+\mathrm{y}^2)^2}$$

Therefore, σ_x induced by distributed force is

$$\sigma_x = -\frac{2}{\pi}\int_{-r}^{r}\frac{qx^3 d\eta}{(\mathrm{x}^2+(\mathrm{y}-\eta)^2)^2}$$

where r is the radius of the hair, and $r = d/2$. According to equations (S5), σ_x is expressed as:

$$\sigma_x = -\frac{2}{\pi}\int_{-r}^{r}\frac{(\frac{0.4}{\pi d^2}+\frac{6.4L}{\pi d^4}\cdot\eta)d\eta}{x(1+(\frac{\mathrm{y}-\eta}{x})^2)^2}$$

$$= -\frac{2}{\pi}\int_{-r}^{r}\frac{-\frac{3.2Lx}{\pi d^4}[2\cdot(\frac{y}{x}-\frac{\eta}{x})]d\eta+(\frac{6.4Ly}{\pi d^4}+\frac{0.4}{\pi d^2})d\eta}{x(1+(\frac{\mathrm{y}-\eta}{x})^2)^2}$$

$$= \frac{6.4Lx}{\pi^2 d^4}\cdot\frac{1}{1+(\frac{\mathrm{y}-\eta}{x})^2}\Big|_{-r}^{r} - \frac{2}{\pi}\int_{-r}^{r}\frac{(\frac{6.4Ly}{\pi d^4}+\frac{0.4}{\pi d^2})d\eta}{x(1+(\frac{\mathrm{y}-\eta}{x})^2)^2}$$

Let $t = \frac{\mathrm{y}-\eta}{x}$, then $\eta = y - tx$, $d\eta = -xdt$.

$$\frac{2}{\pi}\int_{-r}^{r}\frac{(\frac{6.4Ly}{\pi d^4}+\frac{0.4}{\pi d^2})d\eta}{x(1+(\frac{\mathrm{y}-\eta}{x})^2)^2} = \frac{2}{\pi}(\frac{6.4Ly}{\pi d^4}+\frac{0.4}{\pi d^2})\int_{\frac{\mathrm{y}-r}{x}}^{\frac{\mathrm{y}+r}{x}}\frac{dt}{(1+t^2)^2}$$

Let $t = \tan a$, thus $dt = (\sec a)^2\,\mathrm{d}\,a$.

$$\int_{\frac{y-r}{x}}^{\frac{y+r}{x}} \frac{dt}{(1+t^2)^2} = \frac{1}{2}(\sin a\cos a + a)\Big|_{a\min}^{a\max} = \frac{1}{2}\left[t/(t\,\hat{}\,2+1) + \arctan(t)\right]\Big|_{\frac{y-r}{x}}^{\frac{y+r}{x}}$$

Thus, σ_x is expressed:

$$\begin{aligned}\sigma_x &= \frac{6.4Lx}{\pi^2 d^4}\cdot\frac{1}{1+(\frac{y-\eta}{x})^2}\Big|_{-r}^{r} - \frac{1}{\pi}(\frac{6.4Ly}{\pi d^4}+\frac{0.4}{\pi d^2})\left[t/(t\,\hat{}\,2+1)+\arctan(t)\right]\Big|_{\frac{y-r}{x}}^{\frac{y+r}{x}} \\ &= \frac{6.4\gamma x}{\pi^2 d^3}\cdot\frac{1}{1+(\frac{y-\eta}{x})^2}\Big|_{-r}^{r} - \frac{1}{\pi}(\frac{6.4\gamma y}{\pi d^3}+\frac{0.4}{\pi d^2})\left[t/(t\,\hat{}\,2+1)+\arctan(t)\right]\Big|_{\frac{y-r}{x}}^{\frac{y+r}{x}}\end{aligned} \quad \text{(S6)}$$

where the aspect ratio (γ) be defined as L/d. The function relation is made among the stress, diameter and aspect ratio of hair.

Therefore, $\xi_{(x=0.2,y=r)}$ can be expressed as:

$$\begin{aligned}\xi_{(x=0.2,y=r)} &= -\frac{\frac{6.4\gamma\times 0.2}{\pi^2 d^3}\cdot\frac{1}{1+(\frac{y-\eta}{0.2})^2}\Big|_{-r}^{r} - \frac{1}{\pi}(\frac{6.4\gamma r}{\pi d^3}+\frac{0.4}{\pi d^2})\left[5d/(25d\,\hat{}\,2+1)+\arctan(5d)\right]}{\frac{1}{\pi}(\frac{0.4}{\pi d^2})\left[5d/(25d\,\hat{}\,2+1)+\arctan(5d)\right]} \\ &= 1+8\gamma-\frac{16d\gamma}{5d+(1+25d^2)\arctan(5d)}\end{aligned}$$

For a given nylon fiber, d = 0.2 mm, we can obtain

$$\xi_{(x=0.2,y=r)} \approx 1+1.8\gamma \quad \text{(S7)}$$

Note S2. Effect of the Young's modulus of hairs on sensitivity

The hair shaft can be considered as cantilever column under a uniaxial load. The hair shaft is deflected under compression (Fig. S23), and it will return to their initial positions after releasing the applied load. The exact differential equation of the deflection curve is then given by [S1]:

$$\begin{cases} EI\dfrac{d\theta}{ds} = -Fy \\ \dfrac{dx}{ds} = \cos\theta \\ \dfrac{dy}{ds} = \sin\theta \end{cases} \tag{S8 a-c}$$

where θ is the angle between the slope of any point of cantilever column and the x-axis and s is the arc length measured from the free end. The second-order differential equation is given by taking the arc length's derivative of equation (S8a)

$$\frac{d^2\theta}{ds^2} = -\frac{F}{EI}\sin\theta \tag{S9}$$

Let $k^2 = F/EI$, here for a circular cross section, the moment of inertia is $I = \pi d^4/64$, the integration of θ on both sides of equation (S9) gives

$$\frac{1}{2}\left(\frac{d\theta}{ds}\right)^2 = k^2\cos\theta + C \tag{S10}$$

The boundary conditions are:

$$\begin{cases} \dfrac{d\theta}{ds} = 0 \\ \theta = \alpha \end{cases} \tag{S11}$$

By applying the above boundary conditions, we can obtain

$$ds = -\frac{d\theta}{k\sqrt{2}\sqrt{\cos\theta - \cos\alpha}}$$

Finally, we obtain

$$L = \int ds = \frac{1}{2k}\int_0^{\alpha} \frac{d\theta}{\sqrt{\sin^2\dfrac{\alpha}{2} - \sin^2\dfrac{\theta}{2}}}$$

Let $p = \sin(\alpha/2)$, and a new variable φ is introduced and $\sin(\theta/2) = p\sin\varphi$, then we get:

$$L = \frac{1}{k}\int_0^{\pi/2} \frac{d\varphi}{\sqrt{1 - p^2\sin^2\varphi}} = \frac{1}{k}K(p) \tag{S12}$$

where $K(p)$ is complete elliptic integral of the first kind. Then, we can obtain an approximate expression:

$$L = \frac{1}{k} \times \frac{\pi}{2} \frac{1}{(1-0.97p^2)^{1/4}} = \frac{\pi}{2(1-0.97p^2)^{1/4}} \sqrt{\frac{E_f I}{F}} \tag{S13}$$

where E_f is the Young's modulus of hair. Then, we can obtain [S3,S4]:

$$p = \sin\frac{\alpha}{2} = \sqrt{\frac{1-\left(\frac{\pi}{2L}\right)^4 \left(\frac{E_f I}{F}\right)^2}{0.97}} \tag{S14}$$

When the number of hairs is n, then we get

$$p = \sin\frac{\alpha}{2} = \sqrt{\frac{1-\left(\frac{\pi}{2L}\right)^4 \left(\frac{nE_f I}{F}\right)^2}{0.97}} \tag{S15}$$

Meanwhile, $K(p)$=1.8541 can be obtained at $\alpha = \pi / 2$. Considering equation (S12) and $k^2 = F/EI$, we can obtain

$$F = P_{\max} = \frac{nK(p)^2 E_f I}{L^2} \tag{S16}$$

Meanwhile, we can obtain

$$y = \int \sin\theta ds = -\frac{1}{\sqrt{2}k} \int_0^{\alpha} \frac{\sin\theta d\theta}{\sqrt{\cos\theta - \cos\alpha}} = \frac{\sqrt{2}}{k}$$

The aspect ratio (γ) be defined as L/d, where L and d are hair length above the skin substrate and hair diameter, respectively. Thus, we can obtain

$$M_{\max} = P_{\max} y = \frac{\sqrt{2} n\pi K(p) E_f d^3}{64\gamma} \tag{S17}$$

where n = 30 is the number of the hairs. For the given nylon fiber, we can obtain

$$M_{\max} = \frac{6.5}{\gamma} \tag{S18}$$

The aspect ratio (γ) can be obtained from equation (S16).

$$\gamma = \sqrt{\frac{n\pi E_f K^2(p) d^2}{64 P_{\max}}} \tag{S19}$$

For a given operating range F=0~0.1 N, the aspect ratio (γ) of the hairs is estimated to equal 41.3 in terms of formula (S19). Therefore, the fiber length above the skin surface is ca. 7.4 mm.

Note S3. Effect of the Young's modulus of human skin on sensitivity

Hooke law is expressed as [S1]:

$$\varepsilon = \frac{\sigma}{E} \tag{S20}$$

where σ and ε are stress and strain, respectively. E is Young's modulus. For the sensing properties of human skin, the smaller the modulus, the greater the strain, and the more sensitive to external stimuli. A minimum deformation amplitudes (δ_{min}) of about 40 nm can be detected by human skin.[S5] Therefore, the minimum strain (ε_{min}) can be expressed as

$$\varepsilon = \varepsilon_{\min} = \frac{\delta_{\min}}{H} \tag{S21}$$

where H is the thickness of skin and $H \approx 2$ mm. Therefore, the minimum strain (ε_{min}) can be detected is about 2.0×10^{-5}. For human fingertips, the pressure of gentle touch is about 1 KPa.[S6] Therefore, we can obtain:

$$\sigma = E_m \varepsilon_{\min} < 1KPa \tag{S22}$$

where E_m is the modulus of skin. Therefore, we can obtain $E_m < 50$ MPa.

At the same time, the skin needs a certain modulus to protect and buffer the human body and maintain its shape. For human skin, gravity (G) can be expressed as:

$$G = \rho g V$$

where ρ and g are density of skin and gravitational acceleration, respectively. Then, we can obtain:

$$\sigma_G S = \rho g S H$$

where S and H are the area and thickness of skin, respectively. σ_G is stress induced by gravity (see Fig. S24). Therefore, we can obtain:

$$\sigma_G = \rho g H$$

Considering equation (S20), we can get:

$$\varepsilon_G = \frac{\rho g H}{E_m}$$

Therefore, the deformation (δ) of skin under gravity can be expressed as

$$\delta = \int_0^H \varepsilon_G dH = \int_0^H \frac{\rho g H}{E_m} dH = \frac{\rho g H^2}{2E_m} \tag{S23}$$

The average strain ($\overline{\varepsilon}_G$) of the skin under gravity can be expressed as

$$\overline{\varepsilon}_G = \frac{\delta}{H} = \frac{\rho g H}{2E_m} < \varepsilon_{\min} \tag{S24}$$

Therefore, the strain of skin under gravity should be less than ε_{min}. Then, we can obtain:

$$\frac{\rho g H}{2E_m} < 2 \times 10^{-5} \tag{S25}$$

For the human skin, $\rho \approx 1.0 \times 10^3$ kg/m^3, $H \approx 2$ mm, and $g \approx 10$ m/s^2. Therefore, we can obtain $E_m > 0.5$ MPa.

Meanwhile, the mean failure strain [S7] (ε_{max}) of skin is about 50% and the plantar pressure [S8] obtained from barefoot is about 0.1 MPa. In order to ensure that the skin is not damaged, the strain is

$$\varepsilon_{\max} = \frac{\sigma}{E_m} < 0.5 \tag{S26}$$

Therefore, we can obtain $E_m > 0.2$ MPa. According to equations (S22), (S25) and (S26), the modulus of skin ranges from 0.5 MPa ~50 MPa, which is similar to the experimental results for the Young modulus (0.1~18.8 MPa) of human skin.[33] Considering Skin is a highly non-linear material. In the initial loading phase, skin has

very low modulus and large deformation occurs at a relatively low applied load, which will improve the sensitivity of skin.

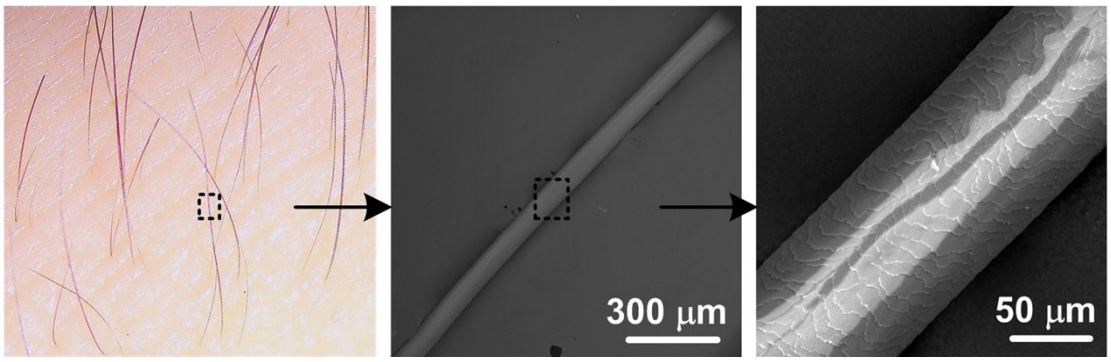

Fig. S1. High magnitude SEM image of one human hair.

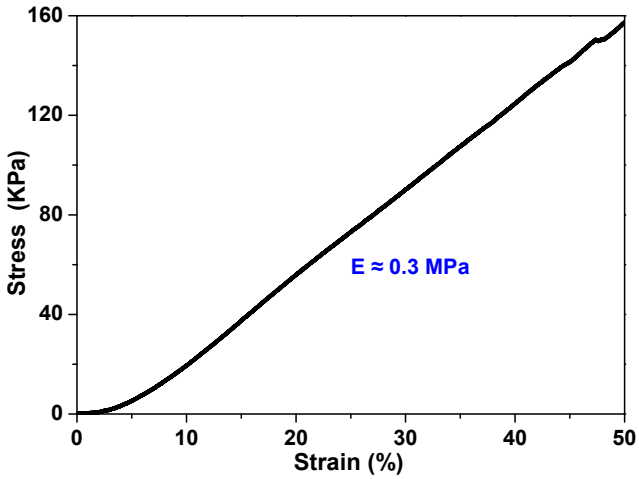

Fig. S2. Stress-strain curve of PDMS. The Young's modulus of PDMS is estimated to be about 0.3 MPa.

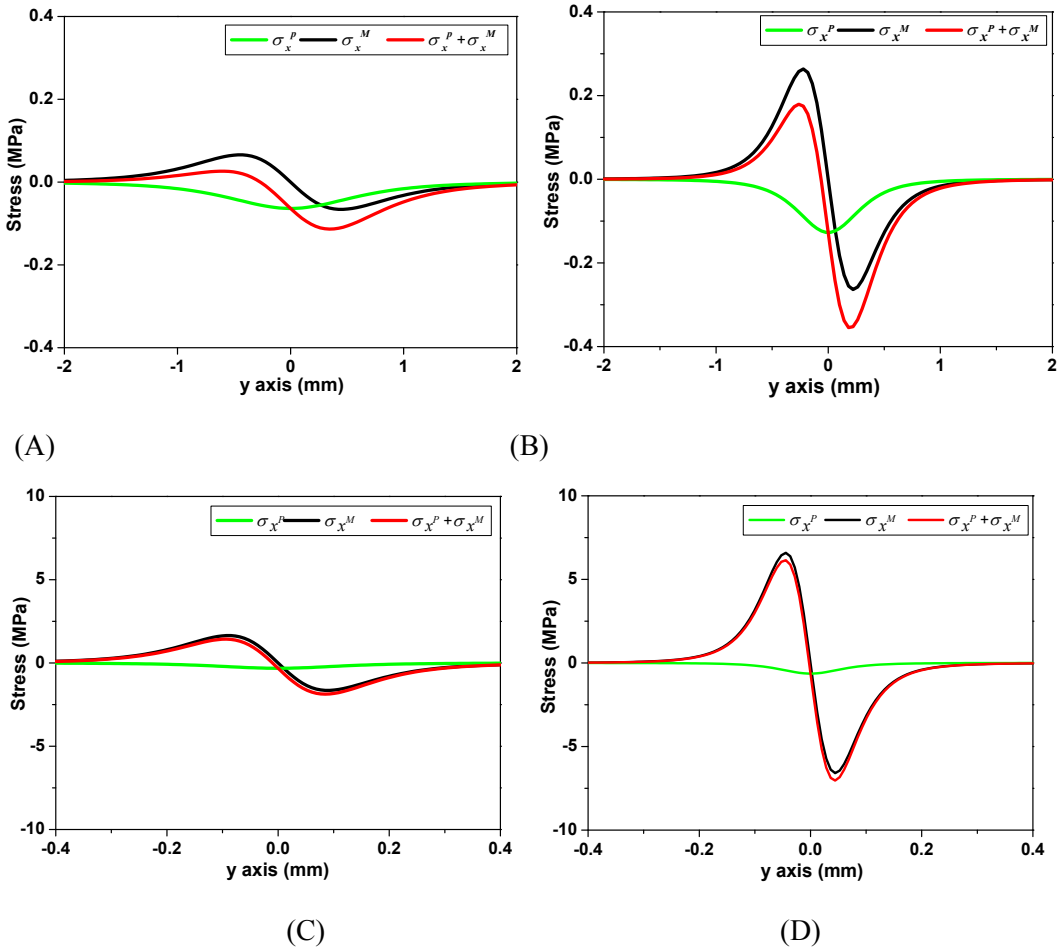

Fig. S3. Stress distributions along y axis. Stresses include σ_x^P (green line) induced by pressure, σ_x^M (black line) caused by moment and their sum of $\sigma_x^P + \sigma_x^M$ (red line). **(A)** x = 1, **(B)** x = 0.5, **(C)** x = 0.2 and **(D)** x = 0.1 mm.

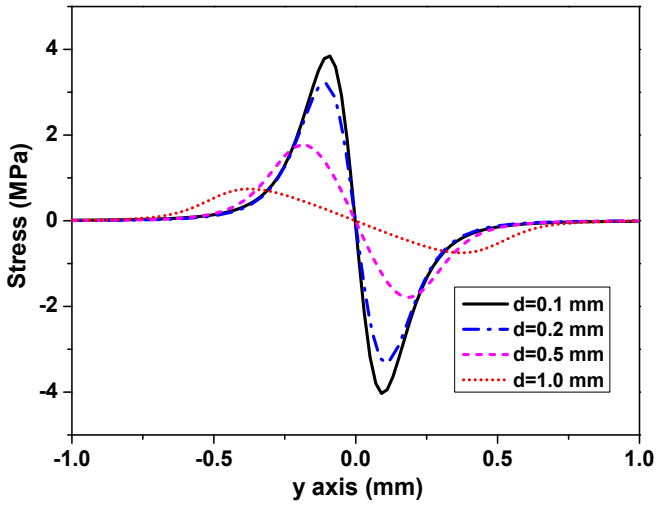

Fig. S4. Dependence of stress ($\sigma_x^P + \sigma_x^M$) on hair diameter. The result was obtained in terms of equation (S4) based on the aspect ratio $\gamma = 41.3$ and $x = 0.2$ *mm*.

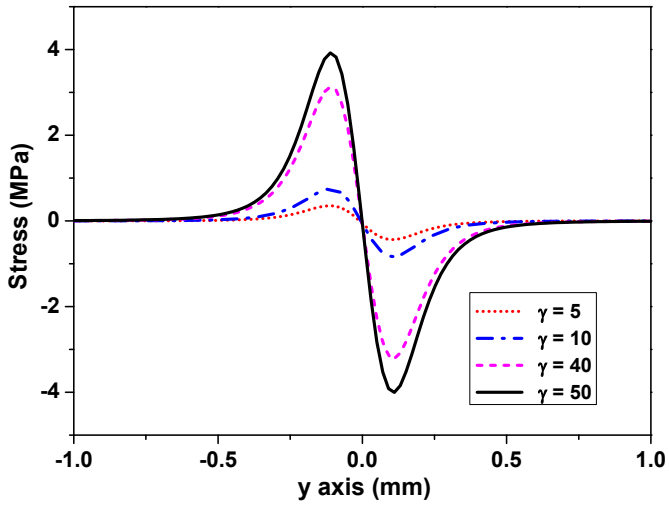

Fig. S5. Dependence of stress ($\sigma_x^P + \sigma_x^M$) on hair aspect ratio. The result was obtained from equation (S4) based on the hair diameter d = 0.2 mm and x = *0.2 mm.*

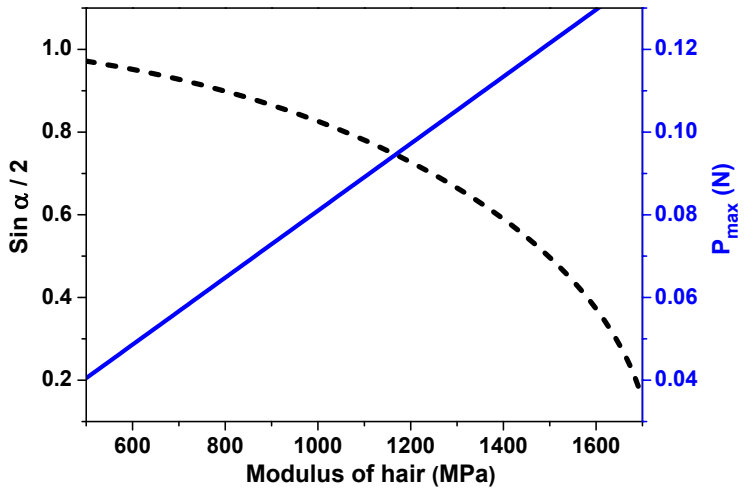

Fig. S6. The angle (α) of hair bending and the maximum force (P_{max}) as a function of Young's modulus (E_f) of hairs. The results were obtained in terms of equations (S15 and S16) based on the number (n = 30) and length L=10 mm of hairs, $I=\pi d^4/64$ and the diameter d = 0.2 mm of hairs. According to equation (S15), the angle (α) of hair bending decreases with increasing the modulus (arbitrary assumption F=0.1 N), which indicates that the lower the modulus, the higher the sensitivity. According to equation (S16), the maximum force (P_{max}) increases with increasing the Young's modulus, which indicates that the higher the modulus, the higher P_{max} is.

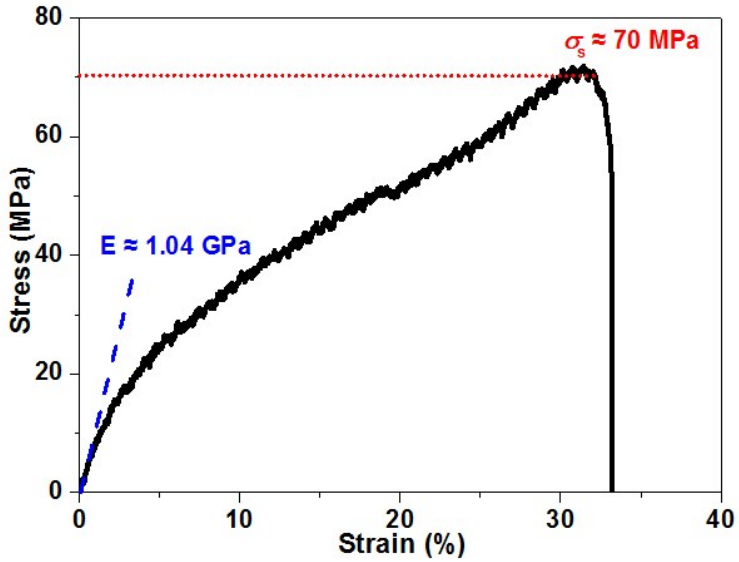

Fig. S7. Stress-strain curve of one nylon fiber as hair material. The nylon fiber is taken from a tooth brush. The Young's modulus and diameter of the nylon hair are 1.04 GPa and 180 μm, respectively, which are close to those of the human hair (E ≈ 0.25~4.2 GPa [35] and d = 30~150 μm [36]).

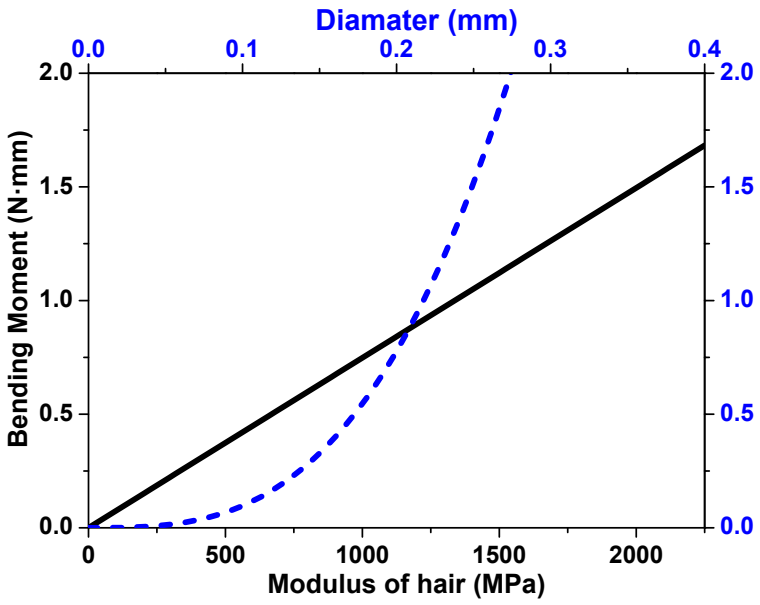

Fig. S8. Dependence of bending moment (N·mm) on diameter and Yong's modulus of hairs. The result was obtained in terms of equation (S17). When E is taken as a variable, d is fixed at 0.2 mm; similarly, when d is a variable, E is fixed at 1.04 GPa.

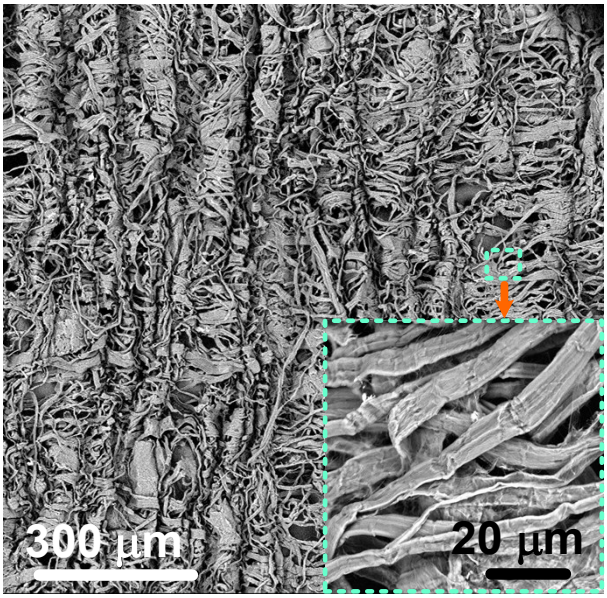

Fig. S9. SEM image of the carbonized paper. Carbonized paper (CP) was prepared through carbonization of single layer tissue paper.

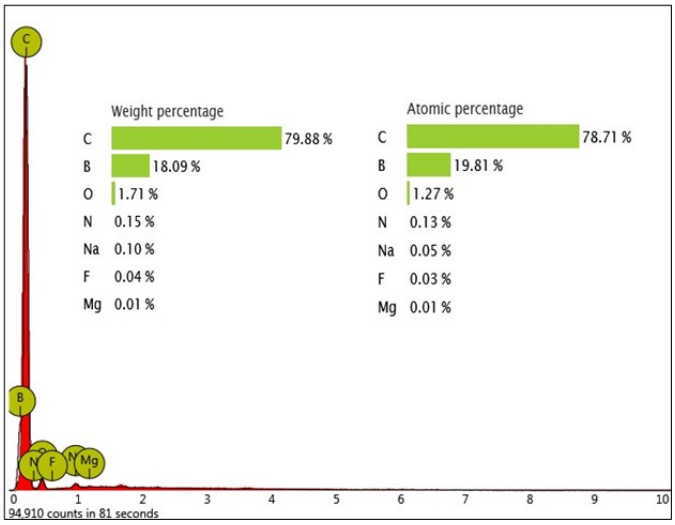

Fig. S10. EDX spectrum of the carbonized paper. EDX results reveal that the elements of C, B, O, N, Na, F and Mg in the carbonized paper are 78.71, 19.81, 1.27, 0.13, 0.05, 0.03 and 0.01 atomic %, respectively. It is obvious that carbon is the dominant element. In addition, the atomic content of Mg, F, N and Na constitutes only 0.22% of the total material, which is normal for carbonized paper obtained from biomass.

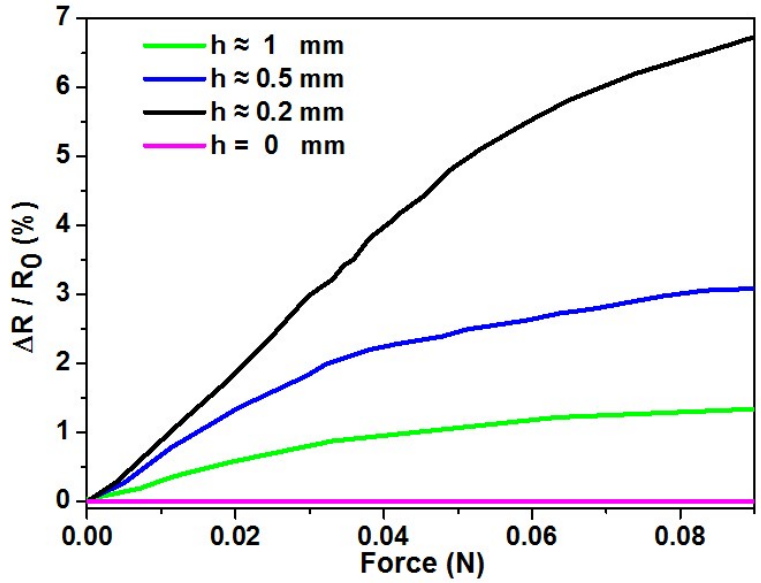

Fig. S11. The RCR response of the EH sensor with different h. h is the distance of the piezoresistive material from the EH surface, and the EH sensor shows the maximum RCR when h = 0.2 mm.

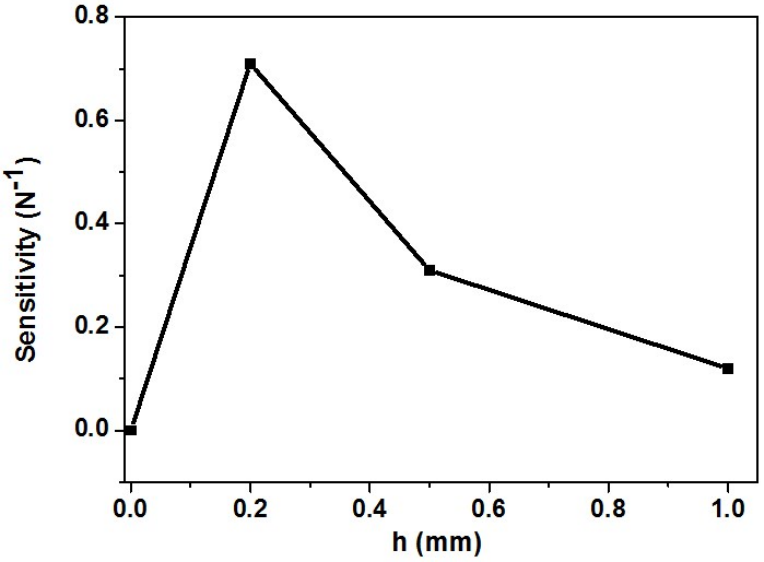

Fig. S12. The sensitivity of the EH sensors with different h. At h = 0.2 mm, the EH sensor shows the highest sensitivity, which is similar to human skin.[31,32]

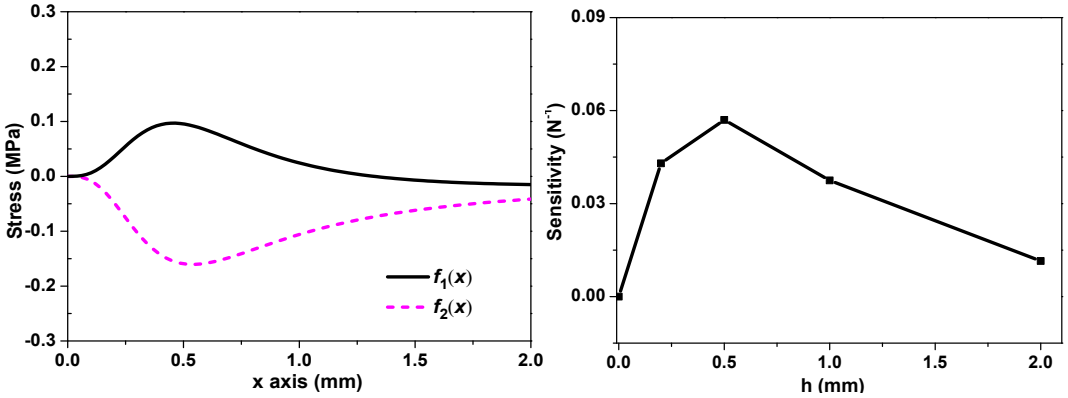

Fig. S13. Theoretical and experimental verification of the maximum stress position along x-axis (y = 0.5 mm). (A) Stress distribution of $f_1(x) = \sigma_x^P + \sigma_x^M$ at y = 0.5 mm and $f_2(x) = \sigma_x^P - \sigma_x^M$ at y = - 0.5 mm along x axis. **(B)** The sensitivity of the EH sensors with different h. At h = 0.5 mm, the EH sensor shows the highest sensitivity.

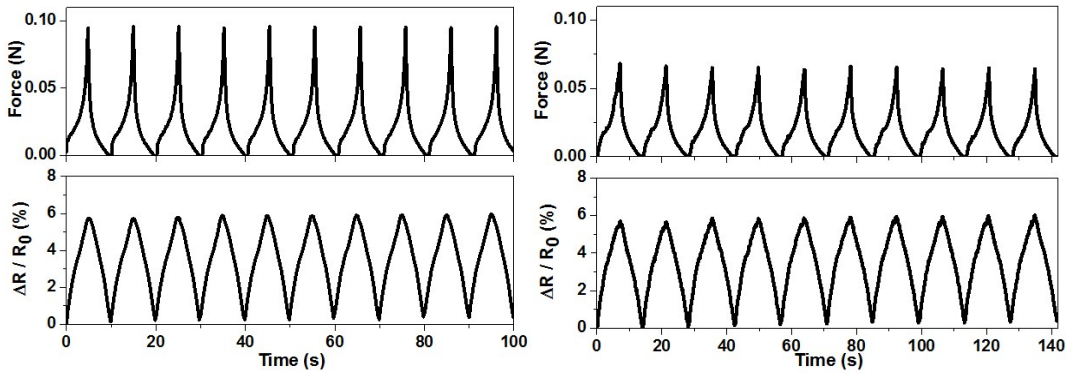

(A) (B)

Fig. S14. The RCR response of the EH sensor monitored by M2. (A) When bending is applied to M1 and **(B)** when cyclic loading is applied to M2.

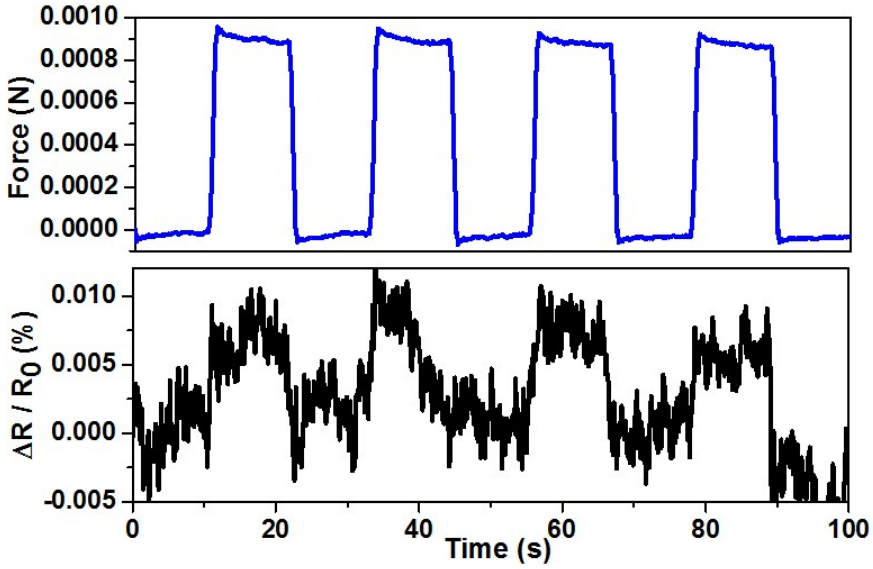

Fig. S15. The RCR response of the EH sensor to a limit force of 1 mN. The results are similar to that (1 mN) of the previous report.[28]

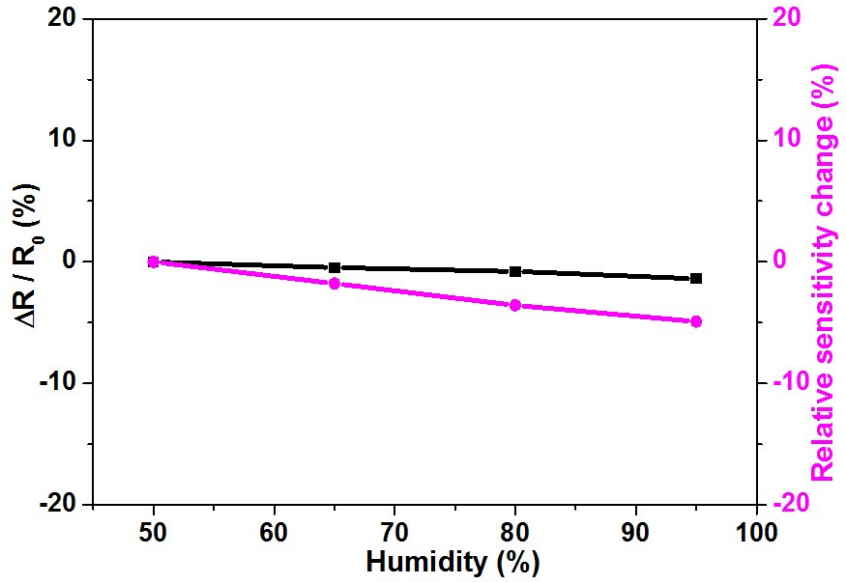

Fig. S16. Effect of humidity on the sensing performance of the EH sensor. When the humidity increases from 50% to 95%, the relative resistance and sensitivity of the EH sensor is reduced by about 1% and 5%, respectively.

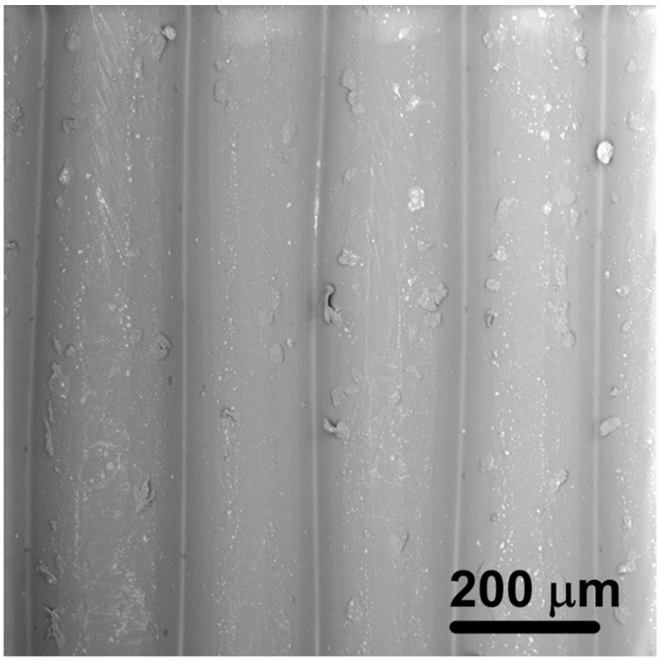

Fig. S17. SEM image of plate A. The roughness is about 200 microns.

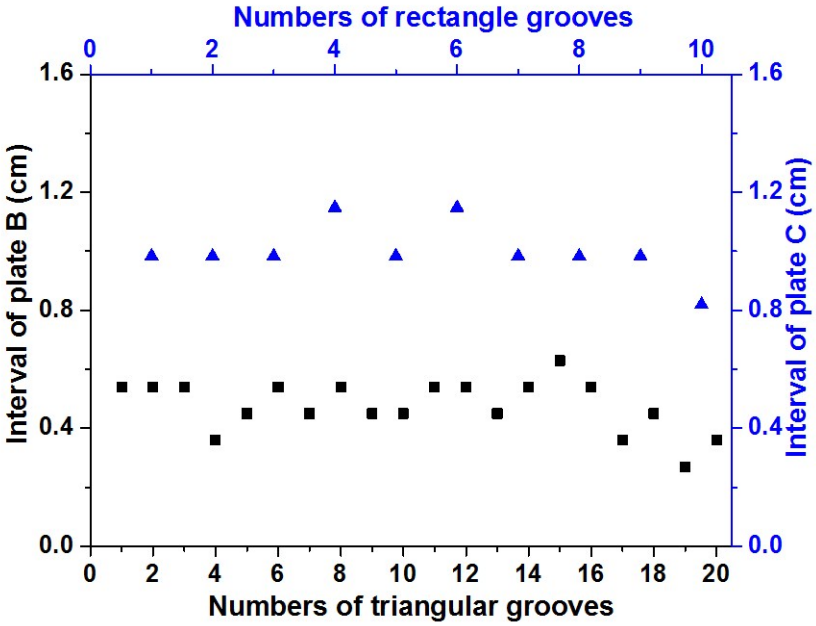

Fig. S18. The interval of grooves in plates B and C. The results are obtained in terms of the RCR curves monitored.

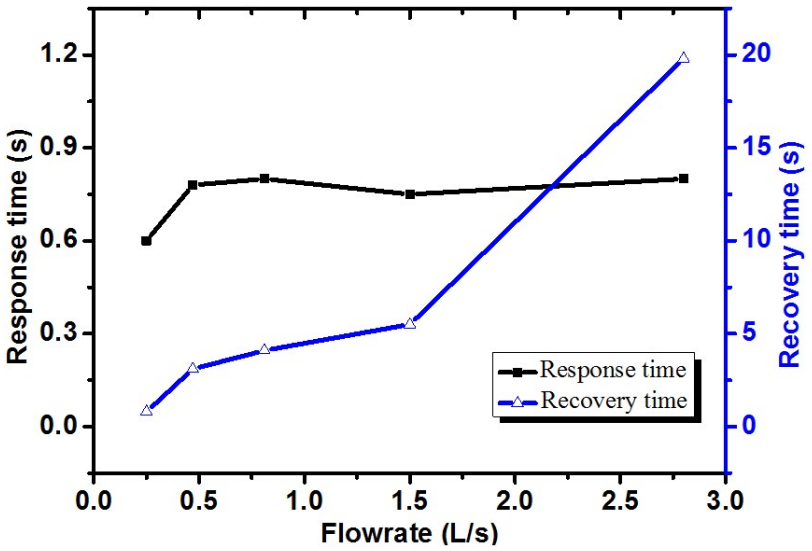

Fig. S19 The response and recovery time of the EH sensor to airflow. Under various air flowrates, the response and recovery time was recorded for the EH sensor.

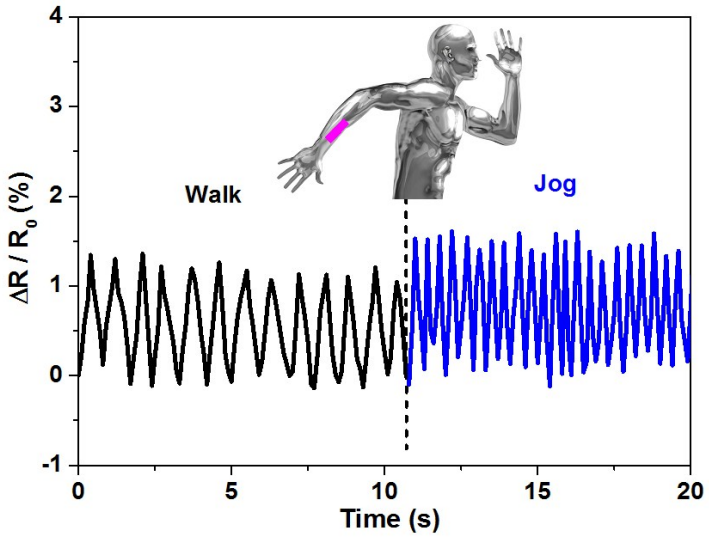

Fig. S20 Response of the EH sensor to walking and jogging. The sensor is fixed on an arm of a man. When the man walks or jogs, the hairs will deform and cause the resistance change of the EH sensor. Thus, the motion signals can be monitored by the EH sensor.

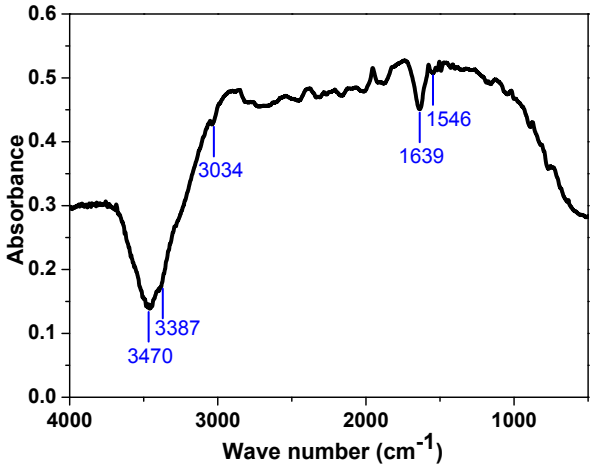

Fig. S21. FT-IR spectrum of nylon fibers. In the frequency range below 1500 cm^{-1} the observed peaks have medium/weak intensities, while in the 1700–1500 cm^{-1} frequency range the observed peaks are strong and are assigned for amide I and II bands. The intense amide I and II bands (namely C-N stretching of amide II band at ~1546 cm^{-1}, C=O stretching vibration of amide I band at ~1639 cm^{-1}) are observed in the frequency range of 1700~1500 cm^{-1}. The bands at ~3034 cm^{-1} and ~3387 cm^{-1} are of special interest because they are related to hydrogen bonding. N-H bending vibration of amide is at ~3470 cm^{-1}. *S9,S10*

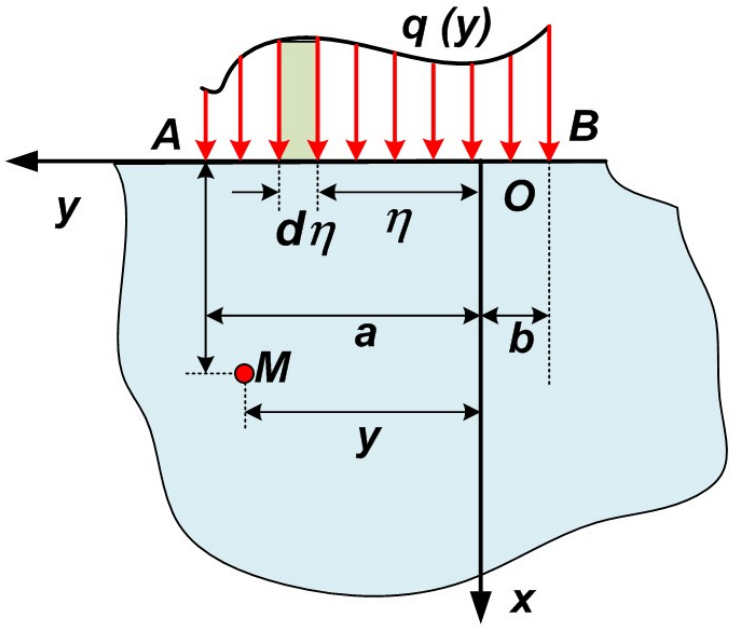

Fig. S22 Half plane under distributed force. Stress distributions are analyzed in the Supplementary Materials.

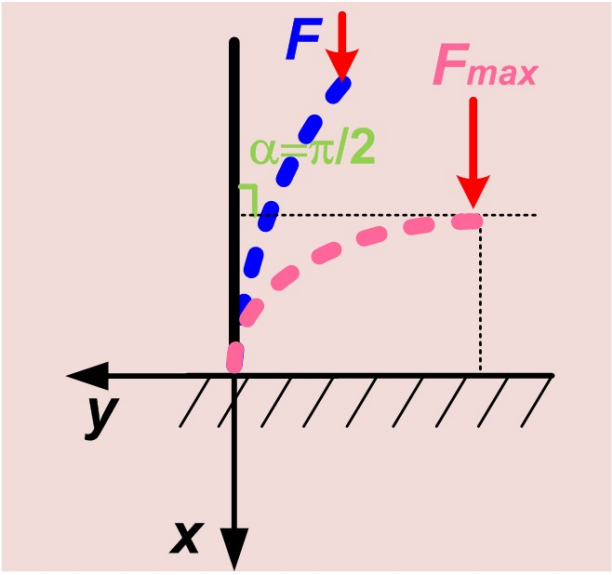

Fig. S23 Schematic showing of hair shaft deformation under an applied force *F*. When $\alpha = \pi/2$, it reaches the maximum working force (F_{max}).

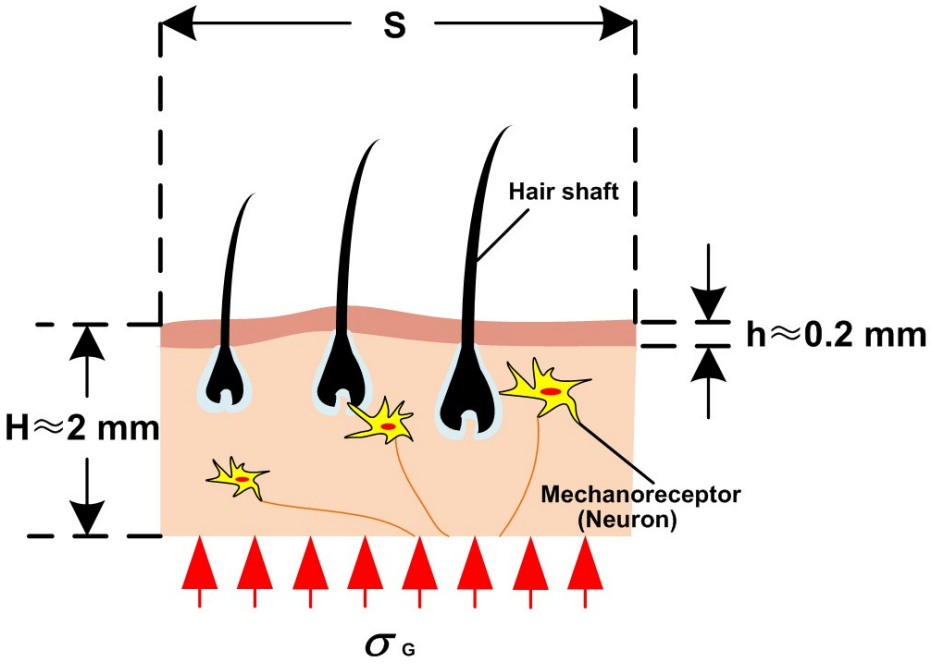

Fig. S24 Schematics of the structure of hair cells and parameters.

Table S1. Comparison of the present EH sensor with existing hair sensors.

Materials	Force Sensitivity (N^{-1})	Roughness (μm)	Airflow Sensitivity (Ω·s /mm)	Resolution (mN)	Air Direction	Ref. No.
Cobalt/SR	0.034~6.9	NA	NA	~ 0.1	NO	28
rGO/HH	0.0049	NA	NA	3000	NO	29
Alloy/SR	0.036	NA	NA	NA	NO	S11
PD/SR	NA	0.5~50	NA	NA	NO	39
CNT/SR	NA	15	NA	NA	NO	S12
Silicon/SR	NA	200	NA	NA	NO	S13
CNT/SR	NA	200	NA	NA	NO	27
rGO/SR	NA	200	NA	~ 1	NO	S14
Graphene/sponge	NA	200	NA	NA	NO	S15
Gold/silicon	NA	NA	~0.079	NA	NO	S16
CB/polyimide	NA	NA	0.066	NA	NO	S17
IN/SR	NA	NA	0.17	~ 0.1	NO	30
Nylon/SR	0.7	200	0.1	~ 1	YES	Present work

Note: NA indicates not available; SR indicates silicone rubber, here is PDMS; rGO indicates reduced graphene oxide; HH indicates human hair; CNT indicates carbon nanotube; IN indicates iron nanowire; PD indicates polyvinylidene difluoride; CB indicates carbon black powder.

It is clear from Table S1 that most of existing hair sensors are either single modular or are not highly sensitive. By the contrary, the present biomimetic multi-responsive EH sensor is not only highly sensible but also capable of detecting multiple signals of pressure, surface roughness and airflow rate/direction, etc. like human shin. It should be pointed out that only in the present work, human skin is fully mimicked by using nylon fibers as hairs and PDMS as human skin. The nylon fibers have similar geometrical sizes, Young's modulus and embedded depth as human hairs in human skin. PDMS as base material for encapsulation of the hair sensor has also similar

Young's modulus as that of human skin. Therefore, it is understandable that the present EH sensor is multi-responsive and highly sensitive to pressure, surface texture and airflow, etc. like human skin.

References

S1. R. D. Specht, *Mathematical theory of elasticity*-2nd ed, McGraw-Hill, **1956**.

S2. E. A. Ripperger, *Mechanics of elastic structures*, Hemisphere Pub. Corp, **1981**.

S3. R. Frisch-Fay, *Int. J. Mech. Sci*, 1963, **5**, 231.

S4. A. R. Vatankhah, *J. Hydrol. Eng*, 2011, **16**, 942.

S5. K. O. Johnson, T. Yoshioka and F. Vega-Bermudez. *J Clin Neurophysiol*, 2000, **17**, 539.

S6. J. Park, Y. Lee, J. Hong, M. Ha, Y. D. Jung, H. Lim, S. Y. Kim and H. Ko, *ACS Nano*, 2014, **8**, 4689.

S7. A. N. Annaidh, K. Bruyère, M. Destrade, M. D. Gilchrist and M. Otténio, *J. Mech. Behav. Biomed*, 2012, **5**, 139.

S8. P. R. Cavanagh, M. M. Rodgers and A. Iiboshi, *Foot Ankle*, 1987, **7**, 262.

S9. Y. Lu, Y. Zhang, G. Zhang, M. Yang, S. Yan and D. Shen, *Polymer*, 2004, **45**, 8999.

S10. N. K. Pramanik, M. S. Alam, R. Kumar and *J. Innov. Resea. Sci. Eng. Tech*. 2015, **04**, 18547.

S11. X. Shi and C. H. Cheng, *The 8th Annual IEEE International Conference on Nano/Micro Engineered and Molecular Systems*, Suzhou, China, April, **2013**.

S12. Y. Cao, T. Li, Y. Gu, H. Luo, S. Wang and T. Zhang, *Small.* 2018, **14**, 1703902.

S13. H. B. Muhammad, C. Recchiuto, C. M. Oddo, L. Beccai, C. J. Anthony, M. J. Adams, M. C. Carrozza and M. C. L. Ward, *Microelectron. Eng.* 2011, **88**, 1811.

S14. S. Chun, H. Jung, Y. Choi, G. Bae, J. P. Kil and W. Park, *Carbon.* 2015, **94**, 982.

S15. S. Chun, A. Hong, Y. Choi, C. Ha and W. Park, *Nanoscale.* 2016, **8**, 9185.

S16. Z. Fan, J. Chen, J. Zou, D. Bullen, C. Liu and F. Delcomyn, *J. Micromech. Microeng.* 2002, **12**, 655.

S17. A. R. Aiyar, S. H. Kim and M. G. Allen. *Smart. Mater. Struct*. 2009, **18**, 447.